Efficient Calculation of Two-Dimensional Adiabatic and Free Energy Maps: Application to the Isomerization of the C13=C14 and C15=N16 Bonds in the Retinal of Bacteriorhodopsin

SERGE CROUZY,[1] JERÔME BAUDRY,[2]* JEREMY C. SMITH,[3] BENOÎT ROUX[4]

[1] *BMC DBMS CEA, 17, rue des Martyrs, 38054 Grenoble cedex 9, France*
[2] *CEA Saclay, France*
[3] *Lehrstuhl für Biocomputing, IWR Universität Heidelberg, Im Neuenheiner Feld 368, D-69120 Heidelberg, Germany*
[4] *Chemistry Department, Université de Montréal, C.P. 6128, succ. A, Montréal, Canada H3C 3J7*

Received 16 April 1999; accepted 6 July 1999

ABSTRACT: Accurate calculation of potential energy and free-energy profiles along reaction coordinates of biological processes such as enzymatic reactions or conformational changes is fundamental to the obtention of theoretical insight into protein function. We describe here the practical implementation of the Automatic Map Refinement Procedure (AMRP) and two-dimensional Weighted Histogram Analysis Method (WHAM) for efficient computation of adiabatic potential energy and free-energy maps, respectively. Methods for efficiently sampling configuration space with high-energy barriers and for removing hysteresis in the case of periodic reaction coordinates are presented. The application of these techniques to the isomerization of the C13=C14 and C15=N16 bonds in the retinal of bacteriorhodopsin is described. In dark-adapted bacteriorhodopsin (bR), the retinal moiety exists in two conformers, *all-trans* and

Correspondence to: S. Crouzy; e-mail: scrouzy@cea.fr
* Present address: Beckman Institute, 405 N. Matthews, Urbana, Illinois 61801

Journal of Computational Chemistry, Vol. 20, No. 15, 1644–1658 (1999)
© 1999 John Wiley & Sons, Inc.
CCC 0192-8651 / 99 / 151644-15

(13,15)cis, with the latter making $\simeq 67\%$ of the population. This experimental free energy difference is reproduced here to within k_BT. © 1999 John Wiley & Sons, Inc. J Comput Chem 20: 1644–1658, 1999

Keywords: free energy; energy minimization; energy map; bacteriorhodopsin; dihedral angle isomerization

Introduction

To describe any given biological conformational change or chemical reaction, it is necessary to choose one or several reaction coordinates ξ, that are able to represent the transformation from ''reactant'' to ''product.'' Depending on the choice of ξ, the barrier height to be overcome along it may vary dramatically. Moreover, although the final free energy difference between ''reactant'' and ''product'' does not theoretically depend on the choice of ξ, in practice, it can affect convergence. Difficulties arise when the configurational sampling around high-energy barriers along ξ is insufficient. This can lead to large-energy differences between forwards and backwards steps along the reaction coordinate (hysteresis) or, in the case of a periodic reaction coordinate such as a dihedral angle, to energy differences between ''reactant'' and, theoretically identical, ''product'' states. This hysteresis may be further increased if a correlation is introduced between adjacent points on the profile, as can be the case if one systematically uses the molecular coordinates obtained in a given simulation at one point as the initial structure for the next.

In the case of potential of mean force (PMF) calculations, $W(\xi)$, the problem of finding the lowest local energy minimum from which to start exacerbates the above-mentioned problem of proper sampling. In previous work[1] we explained how the local energy minimum problem can be overcome by using the Automatic Map Refinement Procedure to efficiently detect energy minima associated with given constrained values of ξ.

Special techniques have been designed to efficiently calculate PMFs from molecular dynamics trajectories. One of these is the umbrella sampling method of Torrie and Valleau.[2,3] In this method, the microscopic system of interest is simulated in the presence of an artificial biasing window potential, $w(\xi)$, introduced to enhance the sampling in the vicinity of a chosen value of ξ. In cases where there is some prior knowledge of the PMF, another way of facilitating the sampling along the reaction coordinate is to add a term that will lower the total barrier experienced from going from ''reactant'' to ''product.'' Assuming that the effect of this potential on $W(\xi)$ can be decoupled from that of the other energy terms, it can be simply subtracted from the final computed map.

Here we examine the above consideration using as a model retinal isomerization in bacteriorhodopsin (bR). BR is the light-driven proton pump protein from the purple membrane of the bacterium *Halobacterium salinarium*.[4] It contains a retinal chromophore covalently linked to lysine 216 via a protonated Schiff base. After absorption by bR of a photon at 568 nm, the retinal undergoes a conformational change that leads to the transfer of a proton from the intracellular to the extracellular side of the membrane. The light-adapted form of bR contains $\simeq 100\%$ *all-trans* retinal (in which all the double bonds of the polyene are in the *trans* conformation). However, after several minutes in the dark, the protein reaches a dark-adapted state. The dark-adapted state has an absorption maximum at 558 nm, and contains a mixture of two isomers of retinal:[5] *all-trans* and *C13=C14 cis, C15=N16 syn*, abbreviated here *(13,15)cis*, in which the dihedral angles C13=C14 and C15=N16 are both *cis*. The two corresponding forms of the protein, denoted bR568 (*all-trans* retinal) and bR548 (*(13,15)cis* retinal), have absorption maxima at 568 and 548 nm, respectively. Results from retinal extraction followed by high-pressure liquid chromatography have led to the suggestion that the bR548 form represents $\simeq 2/3$ of the total.[6,7] The population ratio is modified by changes in temperature, pH, amino acid sequence of bR,[7] and pressure.[8] The retinal isomer composition in membranes treated with Triton X-100, a detergent that gives monomers of bR,[9] is 71% of bR548 at 277 K.[6] The significant population of both forms suggests that the difference in their free energies is inferior to k_BT (where k_B is Boltzmann's constant and T is the temperature).

Important questions remain concerning dark-adapted bR, including the nature of the isomerization pathway from (*all-trans*) to *(13,15)cis* retinal, and the factors influencing the existence of the two forms of bR in the dark-adapted state. Molecular simulation methods can be used to address these questions. Electron cryomicroscopy has been used to obtain an atomic-resolution three-dimensional structure of bR568.[10] This structure is of sufficient accuracy to be useful as the basis for molecular dynamics simulations of the system. Moreover, a comparison can be made with results obtained using a newly available 2.5-Å resolution structure of bR.[11] The present study follows and improves upon previous results on the dark-adapted state of bR,[12] which were obtained from considerations of a limited region only of the relevant dihedral free energy surface.

Theory

The potential of mean force (PMF) $W(\xi)$ along some coordinate ξ, is defined from the average distribution function $\langle \rho(\xi) \rangle$,

$$W(\xi) = W(\xi^*) - k_B T \ln\left[\frac{\langle \rho(\xi) \rangle}{\langle \rho(\xi^*) \rangle}\right] \quad (1)$$

where ξ^* and $W(\xi^*)$ are arbitrary constants. The average distribution function along the coordinate ξ is obtained from a Boltzmann weighted average,

$$\langle \rho(\xi) \rangle = \frac{\int d\mathbf{R}\, \delta(\xi'[\mathbf{R}] - \xi) e^{-U(\mathbf{R})/k_B T}}{\int d\mathbf{R}\, e^{-U(\mathbf{R})/k_B T}}, \quad (2)$$

where $U(\mathbf{R})$ represents the total energy of the system as a function of the coordinates $\mathbf{R}$ and $\xi'[\mathbf{R}]$ is a function depending on a few or several degrees of freedom in the dynamical system.

In the present two-dimensional case, $\xi'[\mathbf{R}]$ will be two dihedral angles, ϕ_1 and ϕ_2.

The presence of large energy barriers along ϕ_1 and ϕ_2 prevents an accurate sampling of the configurational space with presently available computer power using standard MD. To avoid this difficulty, the two-dimensional potential of mean force along ϕ_1 and ϕ_2 is calculated with the umbrella sampling technique of Torrie and Valleau.[2,3] N_w biased distributions are generated using periodic harmonic functions of the form,

$$w_i(\phi_1, \phi_2) = \frac{1}{2} K_1 \left[g(\phi_1 - \phi_1^i) \right]^2 + \frac{1}{2} K_2 \left[g(\phi_2 - \phi_2^i) \right]^2, \quad (3)$$

centered on successive values of ϕ_1^i and ϕ_2^i, where the periodicity is introduced by the function

$$g(\phi) = (|\phi + 180| \bmod 360) - 180 \quad (4)$$

The WHAM equations express the optimal estimate for the unbiased distribution function as a weighted sum over the N_w individual biased distribution functions.[13] The WHAM approach is now routinely used to calculate the PMF along a single coordinate.[14–16] Extensions of the method to multi-dimensional cases is straightforward.[14,15] In the case of the two variables ϕ_1 and ϕ_2, if n_i is the number of independent data points used to construct each biased distribution function

$$\langle \rho(\phi_1, \phi_2) \rangle = \sum_{i=1}^{N_w} n_i \langle \rho(\phi_1, \phi_2) \rangle_{(i)} \times \left[\sum_{j=1}^{N_w} n_j e^{-[w_j(\phi_1, \phi_2) - F_j]/k_B T} \right]^{-1}, \quad (5)$$

where the undetermined constants F_j are defined from,

$$e^{-F_j/k_B T} = \int_{-180}^{180} d\phi_1 \int_{-180}^{180} d\phi_2\, e^{-w_j(\phi_1, \phi_2)/k_B T} \times \langle \rho(\phi_1, \phi_2) \rangle. \quad (6)$$

Because the distribution function itself depends on the set of constants $\{F_j\}$, the WHAM eqs. (5) and (6) must be solved self-consistently. In practice, this is achieved through an iteration procedure. At each step i of the iteration over the N_w windows, the value

$$\mathrm{Diff}^i = \max_j \left\{ |F_j^i - F_j^{i-1}| \right\} \quad (7)$$

is evaluated where F_j^i is the value of F_j in eqs. (5) and (6) at iteration i and j varies from 1 to N_w. The iteration stops when Diff^i is less than a certain tolerance (here 10^{-4}), or when a maximum number of steps has been completed.

Once the 2D free-energy profile $W(\phi_1, \phi_2)$ is obtained, it is straightforward to compute the ratio of equilibrium populations between two conformational states of the protein (S^1, S^2) correspond-

ing to energy wells on the profile by:

$$\frac{P^1}{P^2} = \frac{\int_{\{S^1\}} e^{-W(\phi_1,\phi_2)/k_BT}\, d\phi_1\, d\phi_2}{\int_{\{S^2\}} e^{-W(\phi_1,\phi_2)/k_BT}\, d\phi_1\, d\phi_2} \qquad (8)$$

This measure is far more reliable than the simple Boltzmann ratio of the energies in the two states:

$$\frac{S^1}{S^2} \simeq \frac{e^{-W(\phi_1^1,\phi_2^1)/k_BT}}{e^{-W(\phi_1^2,\phi_2^2)/k_BT}} \qquad (9)$$

APPLICATION TO BACTERIORHODOPSIN (bR)

The above techniques are applied here to the isomerization of the C13=C14 (ϕ_1) and C15=N16 (ϕ_2) bonds in the retinal of bacteriorhodopsin (bR). Three models have been used, model I is retinal linked to LYS216 *in vacuo* and subject to harmonic position restraints,[1] and the two others named II and III, involve retinal inside its explicit protein environment obtained from two available experimental coordinate sets.[10,11]

MODELS AND POTENTIAL FUNCTION

Model I consists of the retinal molecule linked to residue LYS 216 extracted from an experimental structure by Grigorieff et al.[10] The calculations were performed *in vacuo*, with harmonic restraints designed such that the conformational flexibility of the *all-trans* chromophore in the protein is approximately reproduced, as described in detail in our previous work.[1]

The initial coordinates for bR in model II were those used in ref. 17 and derive from the same experimental structure as used for model I.[10] Two hundred, twenty-one residues of bR from ARG 7 to ARG 227 were included in the simulation. Twenty-seven TIP3P[18] water molecules (23 in the hydrophilic part and 4 in the hydrophobic part of the proton transfer channel) were also present, giving a total of 3625 atoms. All hydrogens were present in the model. The water molecules in the hydrophobic channel were placed as in the work of Roux et al.[19]

Model III is a 2.5Å resolution structure of bR that recently became available.[11] We have used this X-ray structure as a starting point for calculating adiabatic and free-energy profiles for rotations around ϕ_1 and ϕ_2. Crystallographic water molecules with B factors less than the average B factor of the protein were included in the calculation. Water molecules close to the retinal Schiff base were not resolved in this structure. As a consequence, bR may not be biologically functional in this model. However, the model allows testing of the influence of the resolution of the initial structure on the calculated energy differences. Results pertaining to model III will be discussed in the section Influence of the initial structure of bR.

The CHARMM program[20] and all-atom potential function[21] were used for the simulations. For both models II and III, aspartic acid residues 96 and 115 were protonated. The force field parametrization of the retinal molecule, residu LYR 216, was described previously.[1,22,23]

The intrinsic dihedral energy terms for rotation around the two double bonds ϕ_1 and ϕ_2 were of the following form:

$$E_\phi(2) = K_\phi(1 + \cos(2\phi - 180)) \qquad (10)$$

As in previous work,[12] $K_{\phi_1} = 3.150$ was used for each of the four dihedral angles representing rotations around C13=C14, namely, C12−C13=C14−C15, C12−C13=C14−H14, C20−C13=C14−C15, and C20−C13=C14−H14, giving a total barrier of 25.2 kcal/mol. $K_{\phi_2} = 3.550$, on the other hand, was used for each of the four dihedral angles representing rotations around C15=N16, namely, C14−C15=N16−CE, C14−C15=N16−H16, H15−C15=N16−CE, and H15−C15=N16−H16, giving a total barrier of 28.4 kcal/mol. To best reproduce results from quantum mechanical calculations, the following two further terms of periodicity one were added:

$$E_{\phi_1}(1) = 0.65(1 + \cos(\phi)) \qquad (11)$$

for ϕ_1 and

$$E_{\phi_2}(1) = 0.51(1 + \cos(\phi - 180)) \qquad (12)$$

for ϕ_2.[1]

Computational Details

For models II and III, we call backbone atoms of bR further than 18 Å away from atom N16 of retinal *far* from the active site. These *far* atoms were weakly restrained to their initial position by a harmonic potential with force constant 2 kcal/(mol · Å^2).[19] Water molecules were confined to remain inside an 18-Å sphere around the same N16 atom by use of the CHARMM boundary

potential.[20,24] The nonbonded interactions were calculated on a group-by-group basis with a cutoff of 13.0 Å. A switching function was applied over 1 Å for both electrostatics and van der Waals interactions. The relative dielectric constant was set to 1. The internal geometry of the TIP3P water molecules and all the bonds involving hydrogen atoms were kept fixed using the SHAKE algorithm.[25,26] An integration time step of 2 fs was used, and Langevin Molecular Dynamics simulations were performed with a friction constant corresponding to a relaxation time of 10 ps^{-1} applied to all nonhydrogen atoms.

Simulations were run on a SGI PowerChallenge and a CRAY T3E at the CEA in Grenoble.

PRACTICAL IMPLEMENTATION

Adiabatic Energy Maps

Adiabatic potential energy maps were calculated for rotations around the two dihedral angles ϕ_1 and ϕ_2 in the whole bR–retinal–water system. The intrinsic double bond dihedral terms [eq. (10)] were set to zero during the minimization, and were subsequently added back to the final map. An initial set of energy minimized structures corresponding to different values of ϕ_1 and ϕ_2 varying from -180 to 180° in steps of 30° (ϕ_{1d} and ϕ_{2d}), was obtained with the protocol defined in flow chart 1a).

The adiabatic maps were then refined with the Automatic Map Refinement Procedure (AMRP), described in detail in our previous work[1] and summarized below. AMRP allows one to automatically refine an adiabatic energy map in CHARMM (or any other program including an energy minimizer). In one dimension, we start with a one-dimensional energy vector representing the energies of N structures obtained for N different values of a reaction coordinate ξ. The program takes as input the list of structure file names and energies ranked in increasing order of ξ from which a list of neighbors to each structure is calculated. Then the energy refinement begins: the program looks for all local minima in the map that have not been used as initial structures for refinement, and energy minimizes each of their two neighbors from the coordinates of the minima. The program checks whether these minima have an energy lower than their newly minimized neighbors. If not, they are refined in the next loop. The loop ends when all points in the map have been used as minima to start the refinement of their neighbors. The procedure can be easily extended to an n-dimensional map by changing the number of neighbors from 2 to $2n$, and also to a periodic map where structures on the ''edges'' and in the ''corners'' are considered as neighbors to one another.

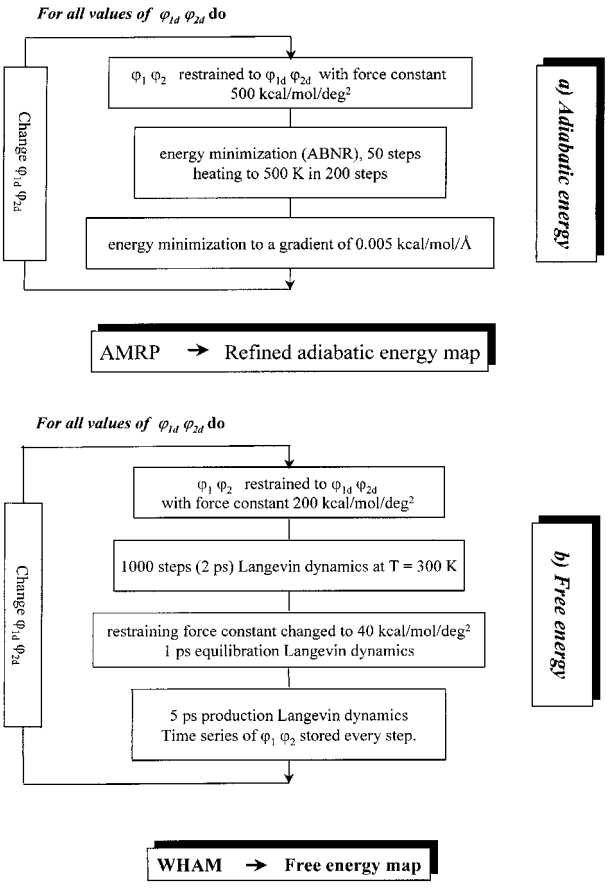

FLOWCHART 1. Flowchart of protocols used for adiabatic (a) and free-energy (b) map calculation. After a first adiabatic map was obtained, AMRP was used to refine it, and the resulting structures used as initial coordinates for (b). Periodic WHAM was used to produce the final free-energy map from the time series calculated in step (b).

Potential of Mean Force Calculation

Strategies to reduce computational cost and remove hysteresis. With the aim of building a 2D free-energy map for rotation around ϕ_1 and ϕ_2, it would seem reasonable to start the sampling from structures yielding an adiabatic map as flat as possible to decrease the computational cost of introducing many umbrella sampling windows to overcome large barriers. Therefore, the intrinsic double bond dihedral terms [eq. (10)] were, as in the case of the

adiabatic profiles, set to zero during the MD then added back in at the end.

Major problems encountered during PMF calculations on large systems, especially when high precision is needed, are unsufficient sampling and hysteresis. In the present work where the reaction coordinates ϕ_1 and ϕ_2 are periodic, a way to enhance sampling involved the cumulation of histograms corresponding to umbrella sampling simulations centered at the same values of (ϕ_1, ϕ_2) modulo 360° and calculated with the same constraining force constants (K_1, K_2). In our previous reports,[1,12] the final hysteresis was removed *a posteriori* by a 2D linear correction. In the present work, we have developed a so-called periodic version of the WHAM program that completely removes the hysteresis. It is clear from eq. (5) and (6) above, that if the biasing potentials [eq. (3)] and the biased distributions $\langle \rho(\phi_1, \phi_2)\rangle_{(i)}$ are periodic, then so will be the unbiased distribution $\langle \rho(\phi_1, \phi_2)\rangle$, the constants F_i and hence the final free-energy profile. As already mentioned, the periodicity of the biasing harmonic potentials was already implemented in CHARMM. The periodicity of the biased distributions was achieved by binning values of the dihedral angles (ϕ_1, ϕ_2) that were less than -180 or more than $+180$° in the histograms at the values $\phi + 360$ or $\phi - 360$°, respectively.

An attempt was made to further flatten the adiabatic energy map by numerically fitting the complete 2D map with simple functions. To obtain a relevant and practical fitting potential, the map obtained with all four internal dihedral angle barriers set to zero (Fig. 2A) was fitted with a sum of cosine and harmonic terms. This new fitted potential was subtracted from the force field and the potential of mean force calculated. In a final step, the fitted potential was added back to the PMF profile. In the ideal case where the fit would be perfect, this procedure would allow the computation of the PMF profile with a single long ''free'' [$K_1 = K_2 = 0$ in eq. (3)] simulation, although such a single simulation may not be a good idea (see ref. 13). The results obtained after the introduction of the fitted potential were very similar to those reported in the next section, which were obtained from the initial map (Fig. 2A) and, therefore, will not be shown.

Umbrella sampling simulations. The $13 \times 13 = 169$ minimized structures obtained after AMRP for ϕ_1, ϕ_2 varying from -180 to 180 in steps of 30° were used as initial coordinates for 2D umbrella sampling molecular dynamics simulations that were performed using the protocol defined in flow chart 1b). During the production dynamics, seven dihedral angles along the retinal backbone were stored, one every 10 steps (20 fs) for further analysis. The average structure and RMS atomic fluctuations during these 5 ps was also calculated.

Our WHAM program allows us to store the biased distributions $\langle \rho(\phi_1, \phi_2)\rangle_{(i)}$ [eq. (5)] and the F_i [eq. (6)] vs. number of iterations. The average values of ϕ_1 and ϕ_2 for each of the previous simulations $(\phi_1^{m(i)}, \phi_2^{m(i)})$ were also calculated. The WHAM procedure also allows one to easily add new time series to further refine a previously calculated PMF. It was found that the biased distribution obtained after the preceding calculation exhibited ''holes'' (nonpopulated bins) for bin widths smaller than 20°. We, therefore, ran several stages of refinement of this first free energy profile introducing new time series so as to permit sampling all the relevant regions of configurational space and to increase the precision of the final profile. This was performed using the following method: (i) the values of the dihedral angles ϕ_1^r and ϕ_2^r corresponding to poorly populated bins (counts less than 10, for instance) were stored, and the values of new biasing potential force constants [K_1 and K_2 in eq. (3)] for a new umbrella sampling run were calculated such that the region of the map around ϕ_1^r, ϕ_2^r would be correctly sampled. The averaged dihedral angle pair $(\phi_1^{m(i_0)}, \phi_2^{m(i_0)})$ closest to (ϕ_1^r, ϕ_2^r) was selected, and the corresponding average structure file i_0 (obtained after step b in flowchart 1) was used as a starting structure for the new run. (ii) After setting the new dihedral restraints corresponding to (ϕ_1^r, ϕ_2^r), 250 steps of ABNR minimization were performed to relieve strains in average structure i_0. New umbrella sampling dynamics followed as described in flow chart 1b).

The refinement was terminated when all bins in the biased distribution were well populated and the F_js reached a plateau before the end of the WHAM iterations.

Results

RETINAL LINKED TO LYS216 IN VACUO: MODEL I

Some results concerning retinal linked to LYS216 *in vacuo* can be found in previous work.[1] In particular, it was found that the *(13,15)cis cis-trans*, *trans-*

cis, and *all-trans* states have potential energies of 4.1, 1.2, 0.0, and 1.7 kcal/mol, respectively. Results of some corresponding Potential of Mean Force calculations with periodic WHAM are summarized in Table I. The results only slightly depend on the bin width used to build the histograms. The Potential of Mean Force map corresponding to a binwidth of 5° is shown in Figure 1. For this bin width, the *cis-trans* and *trans-cis* states are located at $(-5°, 180°)$ and $(175°, -5°)$, with energies of 1.04 and 0.0 kcal/mol, respectively, the latter being the most stable state. Setting $S^1 = trans$ and $S^2 = cis$ in eqs. (8) and (9), the ratio $r = \text{Cis}/(\text{Cis} + \text{Trans})$ was calculated. Results are shown in Table I. For the approximate ratios, energies of the *all-trans* and *(13,15)cis* states are given in the table. The *all-trans* state is more populated than the *(13,15)cis* state, but both are less populated than the *trans-cis* state. Indeed, an integration over each of the four stable states of the free energy map gives (for a bin width of 5°), relative populations of 65.2, 21.6, 12.7, and 0.5% for the *trans-cis*, *all-trans*, *cis-trans*, and *(13,15)cis* states, respectively.

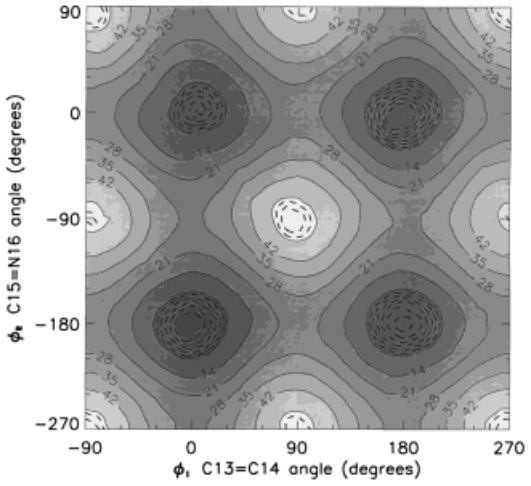

FIGURE 1. Free-energy map for retinal linked to LYS216 *in vacuo* (model I). Free maps are displayed with the Interactive Data Language package,[27] for (ϕ_1, ϕ_2) varying from −90 to 270 degrees for clear visualization of all the energy minima. Maps are interpolated with IDL using triangulation and Akima's quintic polynomials,[28] and the energy minimums set to 0 kcal / mol for display.

RETINAL IN bR: MODEL II

Adiabatic Energy Profiles

For model II of retinal in bacteriorhodopsin, the adiabatic energy map calculated using the Automatic Map Refinement Procedure (AMRP) for rotation around ϕ_1 and ϕ_2 with all intrinsic dihedral energy barriers [eqs. (10), (11), and (12)] set to zero is shown in Figure 2A. This map is almost identical to that published in previous work with shorter refinement.[12] A minimum energy valley located along the ''bicycle pedal'' $\phi_2 = -\phi_1$ diagonal can be seen. The minimum and maximum energy points, 0 and 28.2 kcal/mol are located at $(\phi_1, \phi_2) = (60°, -60°)$ and $(150°, 0°)$, respectively. The maximum results mainly from a combination

TABLE I.
Results of PMF Calculation for Retinal Linked to LYS216 in Vacuo and a Total of 462 Windows.

Bin Width (Degrees)	N_{iter}	(ϕ_1, ϕ_2)*cis* (deg., deg.)	E *cis* kcal / mol	E *trans* kcal / mol	*all-trans* Pop. kcal / mol deg.^{2}	*(13,15)cis* Pop. kcal / mol deg.^{2}	Ratio %	≃ Ratio %
4	1025	(8,4)	2.82	0.59	47	0.7	2.0	2.4
5[a]	1007	(5,5)	2.76	0.64	85	2.1	2.3	2.9
6	978	(6,6)	2.80	0.65	87	2.1	2.3	2.7
9	900	(0,9)	2.60	0.34	178	4.4	2.4	2.3
10	951	(10,0)	3.00	0.36	187	2.3	1.2	1.2
12	836	(12,0)	2.45	0.39	222	6.9	3.0	3.2
15	688	(15,0)	3.33	2.00	21.9	2.2	9.1	10.7

[a]Corresponding to Figure 1.
The number of iterations, N_{iter}, given in the tables correspond to Diff = 10^{-4} in eq. (7). The energy of the *(13,15)cis* and *all-trans* states, after adding the full double-bond intrinsic dihedral energy barriers [eq. (10) with $K_{\phi_1} = 3.15$ and $K_{\phi_2} = 3.55$], are given. The position of the *(13,15)cis* state is also listed (the position of the *all-trans* state being (180,180) for all binwidths). Ratio and ≃ Ratio are the population ratios Cis / (Cis + Trans) calculated with eqs. (8) and (9), respectively. The integration of the energy surface around the energy wells corresponding to the *(13,15)cis* and *all-trans* states, taken as dihedral angles varying in the range [−40,40] and [140,220], respectively, was performed numerically using the function *NIntegrateInterpolatingFunction* of the Mathematica package.[29]

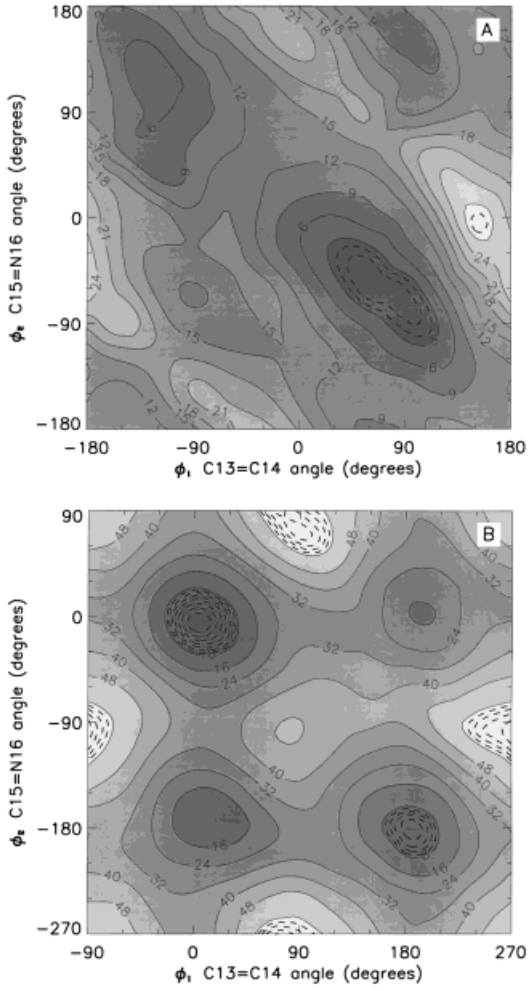

FIGURE 2. (A) Adiabatic energy map for retinal in bR from the experimental structure by Grigorieff et al.,[10] (model II), with all intrinsic dihedral energy barriers [eq. (10), (11), (12)] set to zero. (B) Same map with full intrinsic barriers added.

of relatively unfavorable electrostatic and Van der Waals interactions. The *(13,15)cis* and *all-trans* states have energies of 7.1 and 10.0 kcal/mol, respectively.

After adding back the intrinsic dihedral energy terms, Figure 2B is obtained. The maximum energy of $\simeq 61$ kcal/mol is now located at $(\phi_1, \phi_2) = (-90°, -100°)$. The *(13,15)cis*, *cis-trans*, *trans-cis*, and *all-trans* states are located at $(\phi_1, \phi_2) = (5°, -5°)$, $(15°, -175°)$, $(195°, 0°)$, and $(185°, -180°)$, and have energies of 0.0, 9.5, 14.9, and 3.2 kcal/mol, respectively. These results indicate that the presence of the protein leads to stabilization of the *(13,15)cis* state relative to retinal *in vacuo*. A broader energy well around the *(13,15)cis* state than around the *all-trans* state is clearly visible. The implications of this are further examined, later.

The electrostatic, dihedral angle, and van der Waals contributions to the total energy (Fig. 2A) are shown in Figure 3A, B, and C, respectively. The electrostatic energy is lowest near $(\phi_1, \phi_2) = (0°, -90°)$ at the expense of Van der Waals and internal geometry energy terms (dihedral angle energy in particular), as will be discussed later when characterizing the stable states. Similarly, whereas the electrostatic energy is maximal close to the ''bicycle pedal'' diagonal at $(\phi_1, \phi_2) = (-90°, 60°)$, it is compensated for by a clear Van der Waals energy well in the same region. The dihedral angle energy map contains a valley along the ''bicycle pedal'' diagonal. All other energy terms (not shown) show very little variation upon isomerization of ϕ_1 and ϕ_2. The values of the other retinal dihedral angles during the rotation around ϕ_1 and ϕ_2 were also monitored. Selected dihedrals are shown as a function of C13=C14 and C15=N16 in Figure 4A and B. C13=C14−C15=N16 varies most in the vicinity of the line $\phi_2 = \phi_1$, from $\sim 23°$ for $(\phi_1, \phi_2) = (120°, 90°)$ to 180°. The dihedral potential associated with this single bond rotation (δ) has three minima (2.6 kcal/mol for $\delta = 0°$ or 360° and 3.8 kcal/mol for $\delta = 180°$), separated by two maxima (14.1 kcal/mol for $\delta = 98.4°$ and $\delta = 261.6°$). The energy variation of this term is sufficiently high that it contributes more than 10 kcal/mol to the total energy in the high-energy regions of the adiabatic map.

Along the bicycle pedal diagonal, the dihedral angles C13=C14−C15=N16, N16−CE−CD−CG and CE−CD−CG−CB remain *trans*, while dihedral angles C15=N16−CE−CD and CD−CG−CB−CA have average values of $-64°$ and 80°, respectively, significantly different from their equilibrium geometries of 180° and $(-60, 60, 120)°$, respectively. All other dihedral angles stay close to their equilibrium values during the isomerization of ϕ_1 and ϕ_2. C15=N16−CE−CD goes through a relatively wide range of values ($\simeq 14°$ fluctuation), although its contribution to the total energy is small as its force constant is only 0.3 kcal/mol/rad^2. The harmonic restraints energy term is almost constant (0.7 kcal/mol standard deviation), and does not affect the *(13,15)cis* and *all-trans* populations.

Equilibrium Conformations of Retinal

The four possible (ϕ_1, ϕ_2) equilibrium states of the full bacteriorhodopsin system, *trans-trans*, *trans-cis*, *cis-trans*, and *cis-cis* are now examined in

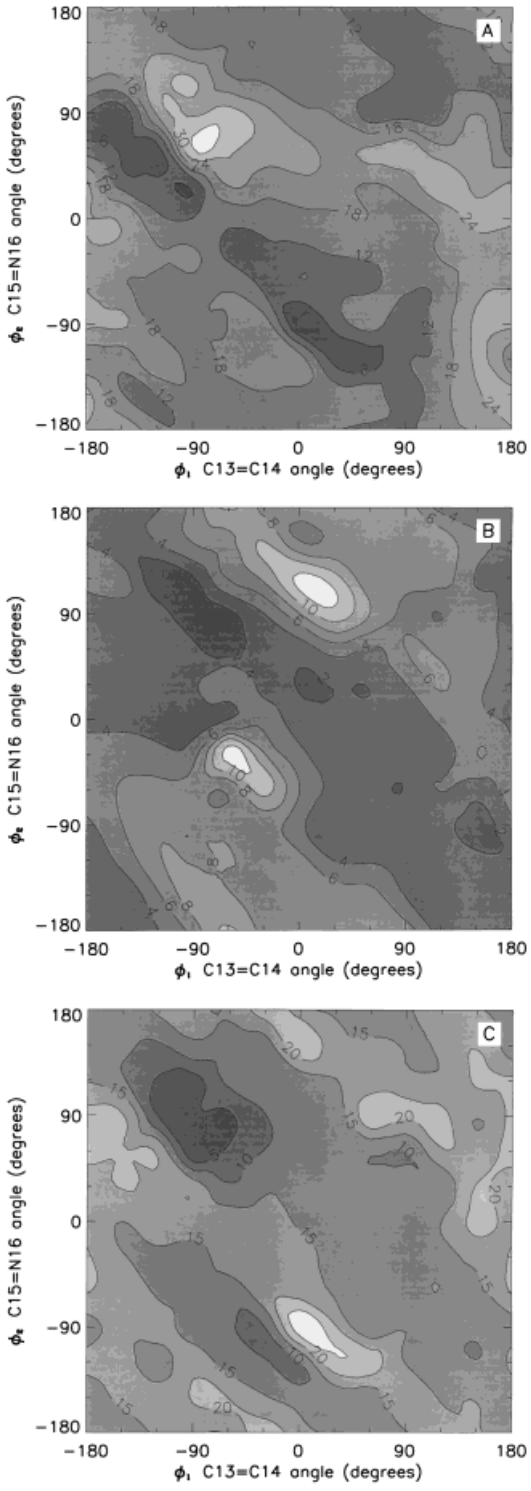

FIGURE 3. Decomposition of the adiabatic energy map for model II into electrostatic (A), dihedral angle (B), and van der Waals energies (C).

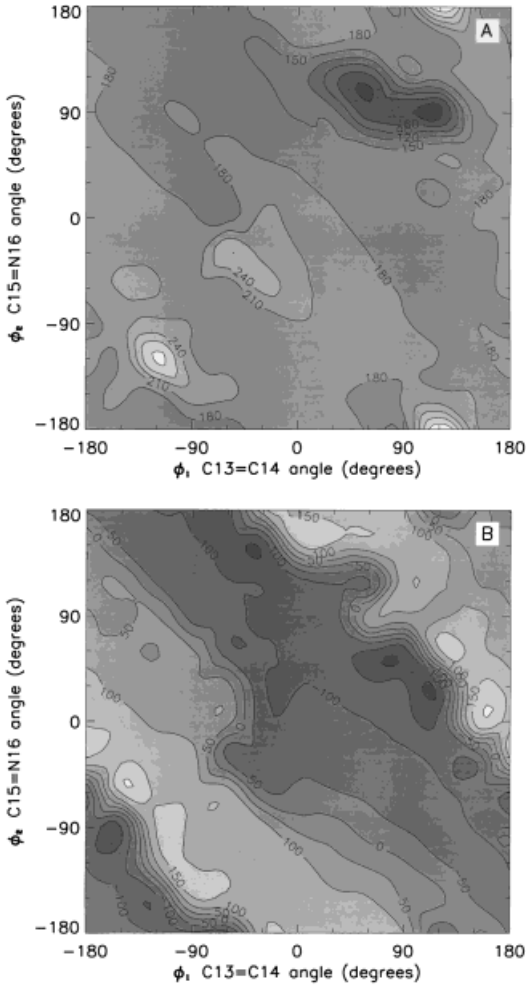

FIGURE 4. C14–C15 (A) and N16–CE (B) dihedral angle maps for model II.

detail. For each state, exhaustive ABNR energy minimization was carried out, starting from the nearest structures obtained after the adiabatic map refinement, down to a gradient of ≤ 0.001 kcal/mol/Å. All intrinsic dihedral barriers for rotations around ϕ_1 and ϕ_2 were included in these minimizations. The results are presented in Table II. The *(13,15)cis* state $(\phi_1, \phi_2) = (6.8°, -3.3°)$ is the most stable, while the *cis-trans* (14.1°, −167.5°), *trans-cis* (−167.2°, 5.4°), and *all-trans* (−174.8°, −179.2°) states have relative energies of 8.2, 14.6, and 2.7 kcal/mol, respectively. The electrostatic energy is lowest in the *cis-trans* state, due to the interaction between water molecules and retinal, described in the next section. In contrast, the internal energy terms are higher in this state than in the others, making it less stable overall. This is especially true for ϕ_1 and ϕ_2, which deviate signifi-

TABLE II.
Equilibrium States of Full Bacteriorhodopsin Water System.

Property	Trans-Trans	Trans-Cis	Cis-Trans	Cis-Cis
Total energy	−3070	−3058	−3064	−3073
Van der Waals energy	−822	−818	−820	−820
Electrostatic energy	−4360	−4359	−4369	−4367
Dihedral angle energy	908	911	914	909
Harmonic energy	249	249	249	249
ϕ_1 = C12−C13=C14−C15	−174.8	−167.2	14.1	6.8
ϕ_2 = C14−C15=N16−CE	−179.2	5.4	−167.5	−3.3
C9=C10−C11=C12	−169.3	−170.6	−172.6	−171.9
C11=C12−C13=C14	177.9	172.4	173.5	178.8
C13=C14−C15=N16	170.9	−170.4	−170.0	−164.1
C15=N16−CE−CD	−59.5	131.8	119.4	−80.5
N16−CE−CD−CG	176.7	64.9	70.5	−173.9
CE−CD−CG−CB	−176.4	−157.7	−169.1	−179.8
CD−CG−CB−CA	75.8	93.9	107.1	89.3

Energies are in kcal / mol, angles in degrees.

cantly from their equilibrium conformations. The dihedral angle N16−CE−CD−CG is in the *gauche* conformation for the *cis-trans* and *trans-cis* states.

Water H-Bonding Network Around Retinal

The H-bonding network of water molecules close to the retinal is shown in Figure 5 for the *all-trans*, *cis-trans*, and *(13,15)cis* conformations of retinal. Following previous work by Nina et al.,[17] four water molecules, labeled 1, 2, 3, and 4, were placed in the hydrophobic channel. In the hydrophilic channel, only the water closest to proton H16 is shown in the figure. The structures of both the residues close to the retinal and of the network of water molecules are almost identical for the *all-trans* and *(13,15)cis* conformations of retinal. The H-bonding network that might play a role in the proton transfer, involves ASP96-W1-W3-W4-LYR and ASP 85. A relatively weak H-bond exists between water W1 and ASP 96. As water W4 makes only one (or two) hydrogen bonds with its environment, one might expect it to be more mobile than waters W2 or W3. In previous modelling, the channel water W2 bridged W1 and W3 in the chain. In the present study it is ejected from the continuous line of four H-bonded waters found by Nina et al.[17] However, with two hydrogen bonds to LYR 216 and THR 46 O atoms, it is very stable, consistent with the experimental observation that it has a low B factor in the crystallographic structure.[11] Moreover, it is an instructive finding of the current work that W2, through the different stages of minimizations and MD simulations translates from its original theoretically examined position to the experimentally observed place. The hydrogen bond between the retinal proton H16 and oxygen OD1 from ASP 85 is the only one broken during the isomerization. This is consistent with Figure 6, which shows the orientation of the vector N16 → H16 with respect to the normal to the bilayer membrane embedding bR. In our previous related work,[12] we defined two possible isomerizations pathways for retinal: the bicycle pedal diagonal (A) and *all-trans−cis-trans−(13,15)cis* (B). It is instructive to notice that our simulations predict that following the bicycle pedal diagonal (A), H16 constantly points towards the extracellular medium (ASP 85) whereas, following pathway (B), H16 first points towards the extracellular medium (ASP 85) then towards the cytoplasmic side (ASP 96) at the *cis-trans* intermediate, and finally back towards the exterior of the cell in the *(13,15)cis* state.

Free-Energy Profiles and Population Analysis

As described in section Practical Implementation, the PMF for rotations around (ϕ_1, ϕ_2) were calculated starting from minimized structures obtained with AMRP. Results of the Potential of Mean Force calculations and the corresponding population ratios are shown in Table III. The Potential of Mean Force map corresponding to a binwidth of 5°, is shown in Figure 7. Results are close to experimental values with a ratio less than 90%, and are very similar for binwidths less or

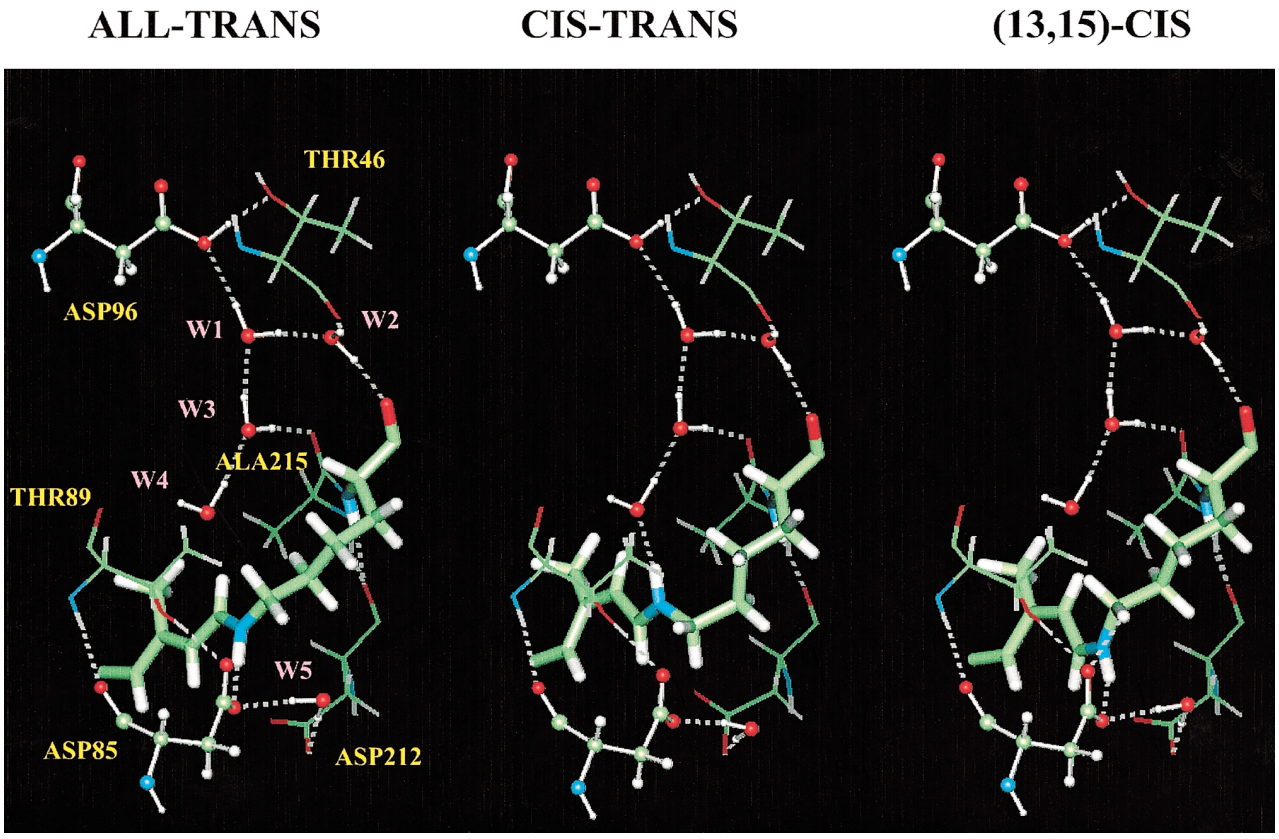

FIGURE 5. Water H-bonding network around retinal for the *all-trans, cis-trans,* and *(13,15)cis* equilibrium conformations, derived from model II.

equal to 6°. The population ratios calculated from the approximate equation [eq. (9)] are close to those obtained with complete integration over the energy wells [eq. (8)].

The values of the force constants for the intrinsic torsional terms are not known accurately, and vary even more when a negative charge is located close to the Schiff base (see ref. 12 for details). Recent *ab initio* calculations by Logunov and Schulten[30] for a corotation of C13=C14 and C15=N16, strictly following the bicycle pedal diagonal, give a barrier of 22 kcal/mol in the case of a protonated Asp85 residue. We used this barrier height, corresponding to $K_{\phi_1} = K_{\phi_2} = 1.88$ kcal/mol in our previous work[12] to investigate the role of the barrier on the two possible isomerization pathways, from adiabatic energy maps. Here, we calculate the barrier height that would make the two isomerization pathways (A) and (B) approximately equiprobable. From the previous free

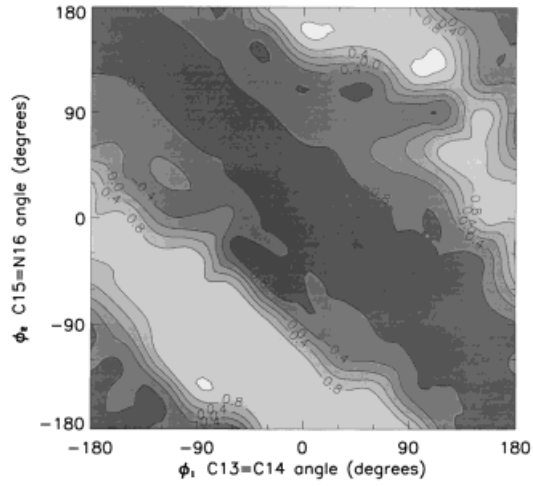

FIGURE 6. Orientation of the N16−H16 vector in retinal derived from model II. Orientations close to 1 or −1 mean that the vector N16 → H16 is close to normal to the membrane plane, positive values meaning the vector is oriented in the direction from ASP 85 to ASP 96.

TABLE III.
Results of PMF Calculation from the bR Structure by Grigorieff et al. (model II) with 587 Windows.

Bin Width (Degrees)	N_{iter}	(ϕ_1, ϕ_2)*cis* (deg., deg.)	(ϕ_1, ϕ_2)*trans* (deg., deg.)	E *trans* kcal / mol	*all-trans* Pop. kcal / mol deg.^{2}	*(13,15)cis* Pop. kcal / mol deg.^{2}	Ratio %	≃ Ratio %
3	2671	(6, − 3)	(183,177)	1.18	22.0	178	89.0	87.8
4	2580	(8, − 4)	(184,176)	1.45	15.1	164	91.5	91.9
5[a]	2489	(5, − 5)	(185,175)	1.26	24.2	232	90.5	89.2
6	2326	(6, − 6)	(180,174)	1.80	13.4	229	94.5	95.3
9	2198	(9,0)	(189,180)	1.25	40.9	301	88.0	89.1
10	2176	(10,0)	(180,180)	1.08	56.7	320	85.0	86.0
12	1949	(12,0)	(180,180)	2.07	15.1	397	96.3	97.0
15	2136	(15,0)	(180,180)	4.30	0.4	525	99.9	99.9

The energy of the *(13,15)cis* state, whose position is given in the table, is 0 kcal / mol after adding the full double-bond intrinsic dihedral energy barriers [eq. (10) with $K_{\phi_1} = 3.15$ and $K_{\phi_2} = 3.55$].

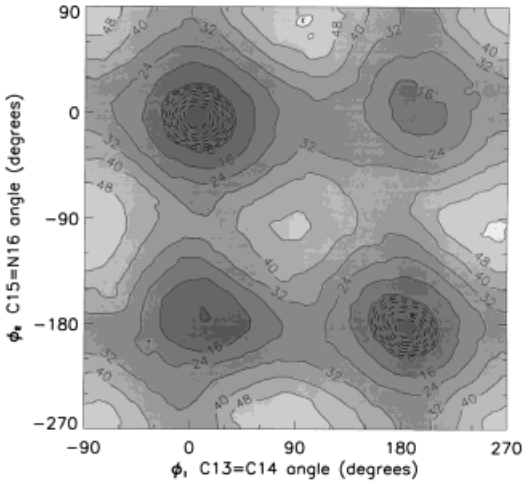

FIGURE 7. Free-energy map for rotations around the two dihedral angles ϕ_1 and ϕ_2 in the whole bR−retinal−water system (model II) and with full intrinsic barriers [eq. (10) with $K_{\phi_1} = 3.15$ and $K_{\phi_2} = 3.55$].

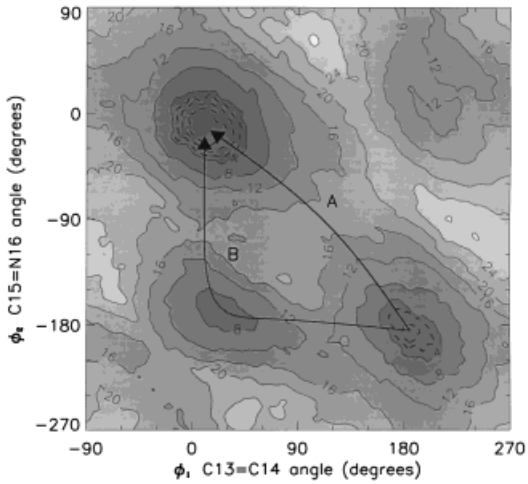

FIGURE 8. Free-energy map for model II with reduced double-bond intrinsic dihedral energy barriers [eq. (10) with $K_{\phi_1} = K_{\phi_2} = 1.35$ kcal / mol]. The two possible isomerization pathways (A) and (B) are highlighted.

energy map (Fig. 7), this barrier height is estimated at 14.6 kcal/mol from the *all-trans* state to the barrier top around $(\phi_1, \phi_2) = (90°, -90°)$. This reduced energy barrier corresponding to $K_{\phi_1} = K_{\phi_2} = 1.35$ kcal/mol was used to draw the map shown in Figure 8 with pathways A and B highlighted.

The variation of the results with the number of WHAM iterations was also examined, to check whether the WHAM program had converged. If we analyze the WHAM convergence in detail, we find that, for a fixed bin width of 5° and a tolerance [final value of Diff defined in eq. (7)] of 10^{-6}, the F^j in eq. (6), themselves, converge at varying rates. The 14 slowest to converge are shown in Figure 9. The corresponding values of Diff are shown in Figure 10. After a very fast decrease of Diff during the first 500 iterations or so, the number of steps needed to lower Diff further increases almost exponentially. From Figures 9 and 10, we see that around 2000 iterations are needed to attain convergence of all the F^j, which corresponds to a final tolerance around 10^{-4}, the value that was used for the results presented in Tables III and V. The Cis/(Cis + Trans) ratios in dark-adapted bR were found to vary only slightly as a function of the tolerance for this same binwidth of 5°. For the whole range of tolerances from 0.01 (where the F^j, clearly, have not all converged) to 10^{-6} the ratios

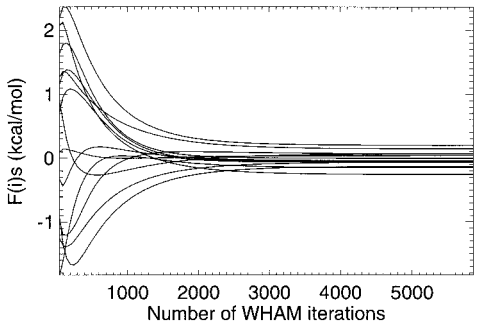

FIGURE 9. Plot of the 14 most slowly convergent F^j [eq. (6)] calculated for model II with a binwidth of 5° and a tolerance [final value of Diff, eq. (7)] of 10^{-6}.

vary only from 89.5% to 90.5%. Therefore, this particular result is not very sensitive to a perfect convergence of WHAM.

INFLUENCE OF THE INITIAL STRUCTURE OF bR: MODEL III

The adiabatic energy map obtained from the new structure,[11] corresponding to model III, is very similar to that shown in Figure 2B. As in Figure 2B, the *(13,15)cis* state ($(\phi_1, \phi_2) = (0°, -5°)$) is the most stable while the *cis-trans* (20°, −150°), *trans-cis* (210°, 20°), and *all-trans* (185°, −180°) states have relative energies of 17.6, 18.5, and 3.7 kcal/mol, respectively. A significant increase in the relative energies of the *cis-trans* and *trans-cis* states, relative to model II, is, however, observed. We now examine the behavior of the crystallographic water molecules from ref. 11, closest to the retinal. Comparison with model II shows that one water corresponds to W5 of model II and another to W2. The three other crystallographic water molecules labeled 5, 6, and 7 in ref. 11 are close to water molecules W1, W3, and W4 in the present work.

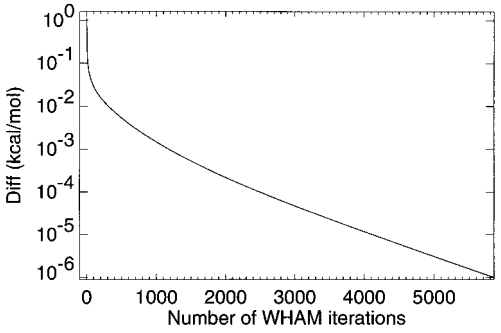

FIGURE 10. Typical evolution of Diff [Eq. (7)] with the number of WHAM iterations.

TABLE IV.
Water H-Bonding Network from the bR Structure by Pebay – Peyroula et al. (Model III).

H-Bond	$\langle d \rangle$	σ_d
HE1 TRP182 — OH2 W′1	1.95	0.05
H1 W′1 — OG1 THR178	2.13	0.20
H1 W′2 — O LYR216	2.25	0.57
H2 W′2 — O THR46	2.00	0.15
H1 W′3 — OD2 ASP212	2.39	0.78
H1 W′3 — OD1 ASP85	2.84	0.06
H2 W′3 — OD1 ASP85	1.69	0.05
HE1 TRP86 — OH2 W′3	2.63	0.16
H2 W′4 — OH2 W′3	1.81	0.05

Crystal-lographic water molecules are labeled W′1, W′2, W′3, and W′4.

The two-dimensional potential of mean force starting from the new bR structure, model III, was calculated with exactly the same protocol as for model II. The results are reported in Table V. These results are similar to those presented in detail in Table III, although slightly closer to the experimental values. The *cis* state is still slightly

TABLE V.
Results of PMF Calculation from the bR Structure by Pebay – Peyroula et al. (model III) with 394 Windows.

Bin Width (Degrees)	N_{iter}	(ϕ_1, ϕ_2)*cis* (deg., deg.)	(ϕ_1, ϕ_2)*trans* (deg., deg.)	E *trans* kcal / mol	*all-trans* Pop. kcal / mol deg^2	*(13,15)cis* Pop. kcal / mol deg^2	Ratio %	≃ Ratio %
4	2749	(4, − 4)	(180,176)	0.76	51.3	260	83.5	78.2
5	2693	(5, − 5)	(180,175)	0.75	61.4	278	81.9	77.8
6	2538	(0, − 6)	(180,174)	0.92	53.6	270	83.4	82.4
9	2157	(0, − 9)	(180,180)	1.58	23.0	358	94.0	93.4
10	2380	(0, − 10)	(180,180)	0.95	71.7	394	84.6	83.1
12	2513	(0, − 12)	(180,180)	2.00	13.1	480	97.3	96.6
15	3314	(0, − 15)	(180,180)	0.85	125	449	78.2	80.6

more densely populated with respect to the *trans* state than found experimentally (ratio ≃ 67%).

Discussion and Conclusion

The present work examines practical aspects of PMF calculations with the iterative Weighted Histogram Analysis Method, using as an example application to the retinal isomerization. WHAM has been described as an accurate method for computing free energy profiles along simple reaction coordinates.[13] In the present application, the method is extended to two dimensions. Furthermore, WHAM is combined here with the Automatic Map Refinement Protocol. The AMRP protocol yields maps that exhibit the following properties: (1) The $2N$ (where N is the dimensionality of the problem) neighboring structures [where neighbor means obtained for successive values of the reaction coordinate(s)] conserve a correlation between them because any one structure is obtained by energy minimizing neighbors. This ensures smoothness of the map. (2) Two distant structures may stay uncorrelated. This is because initial structures for AMRP may come from minimizations where the value of a reaction coordinate is increased gradually, from molecular dynamics simulations with free or constrained reaction coordinates, from simulated annealing protocols or from combinations of the above. This is in contrast to calculations where structures are obtained from a gradual increase of the reaction coordinate only. In such calculations, increasing the value of the reaction coordinate often results in a slowly increasing perturbation of another degree of freedom in the system (very often an improper angle energy term) until this other degree of freedom suddenly overcomes a barrier and falls into another local minimum. The new structure then has an energy much lower than the previous one.

A consequence of the continuity of the AMRP maps is that PMF maps derived from them also tend to be smooth: no abrupt energy peaks. When the umbrella biasing potential is periodic with respect to the reaction coordinate, use of a periodic WHAM allows the calculation of periodic free energy profiles with no hysteresis.

With the tuned energy minimization and PMF calculation protocols, we have been able to extract interesting information on the equilibrium states and possible proton-pumping mechanism of bacteriorhodopsin. The structures of these equilibrium states of retinal result from the adiabatic map calculation. As a result of the use of AMRP, their energies are much lower than when obtained by direct minimization of the crystal structure. The *(13,15)cis*, *cis-trans*, *trans-cis*, and *all-trans* states have relative potential energies of 0.0, 8.2, 14.6, and 2.7 kcal/mol, respectively. The same stable states have relative free energies (measured on the 3° bin width map built from model II) of 0.0, 7.8, 11.4, and 1.2 kcal/mol, respectively. This corresponds to an entropic stabilization of the *(13,15)cis* state of about 1.5 kcal/mol and improved agreement with the experimental result of roughly 0.5 kcal/mol free-energy difference between the two states. With model III, this free-energy difference is further reduced, to 0.76 kcal/mol (for a binwidth of 4°), very close to the experimental value.

Given the necessary number of steps required to obtain stable values for all F^js, and the exponential increase in computational cost with the number of steps, a tolerance value of 10^{-4} kcal/mol for a WHAM calculation seems optimal in the present case. Adiabatic and free energy maps (Figs. 2B and 7) superimpose very well, which shows that the entropic contribution to the free energy profile is small. However, inside the minimum energy wells, important differences are detected. It is clear from Table VI that the population ratio *(13,15)cis / ((13,15)cis + all-trans)* in the protein is significantly higher when calculated from the adiabatic map than from the potential of mean force map. Using the above-recommended tolerance and a small bin width to build the histograms (3 or 4° in Table VI), a ratio around 80% in favor of the *(13,15)cis* state of retinal is obtained from the free energy profile, in excellent agreement with experiment. This ratio also agrees with our previous study via the ''bicycle pedal'' pathway,[12] where a value of 76% in favor of the *(13,15)cis* state was found. The results presented here depend only slightly on the experimental initial structure of the protein used. Furthermore, the

TABLE VI.
Comparison between Population Ratios Obtained from Adiabatic and Free-Energy Maps.

Model	Cis / (Cis + Trans) (AMRP) %	Cis / (Cis + Trans) (PMF) %
I	2.6	2.4
II	99.5	87.8
III	99.7	78.2

population ratio obtained with retinal linked to LYS216 *in vacuo* are qualitatively the opposite to those found experimentally in bR, confirming that the protein environment around retinal is fundamental to its function.

References

1. Baudry, J.; Crouzy, S.; Roux, B.; Smith, J. C. J Chem Inf Comp Sci 1997, 37, 1018.
2. Torrie, G. M.; Valleau, J. P. Chem Phys Lett 1974, 28, 578.
3. Valleau, J. P.; Torrie, G. M. Statistical Mechanics, Part A; Berne, J., Ed.; Plenum Press: New York, 1977.
4. Oesterhelt, D.; Stoeckenius, W. Nat New Biol 1971, 233, 149.
5. Harbison, G. S.; Smith, S. O.; Pardoen, J. A.; Winkel, C.; Lugtenburg, J.; Herzfeld, J.; Mathies, R.; Griffin, R. G. Proc Natl Acad Sci USA 1984, 81, 1706.
6. Scherrer, P.; Mathew, M. K.; Sperling, W.; Stoecknius, W. Biochemistry 1989, 28, 829.
7. Song, L.; Yang, D.; El-Sayed, M. A.; Lanyi, J. K. J Phys Chem 1995, 99, 10052.
8. Schulte, A.; Bradley, L., II. Appl Spectrosc 1995, 49, 80.
9. Massote, D.; Aghion, J. Biochem Biophys Res Commun 1991, 181, 1301.
10. Grigorieff, N.; Cesta, T. A.; Downing, K. H.; Baldwin, J. M.; Henderson, R. J Mol Biol 1996, 259, 393.
11. Pebay−Peyroula, E.; Rummel, G.; Rosenbusch, J. P.; Landau, E. M. Science 1997, 277, 1676.
12. Baudry, J.; Crouzy, S.; Roux, B.; Smith, J. C. Biophys J 1999, 76, 1909.
13. Roux, B. Comput Phys Commun 1995, 91, 275.
14. Kumar, S.; Bouzida, D.; Swendsen, R. H.; Kollman, P. A.; Rosenberg, J. M. J Comp Chem 1992, 13, 1011.
15. Boczko, E. M.; Brooks III. C. L. J Phys Chem 1993, 97, 4509.
16. Brooks III C. L.; Nilsson, L. J Am Chem Soc 1993, 115, 11034.
17. Nina, M.; Roux, B.; Smith, J. C. Biophys J 1995, 68, 25.
18. Jorgensen, W. L.; Impey, R. W.; Chandrasekhar, J.; Madura, J. D.; Klein, M. L. J Chem Phys 1983, 79, 926.
19. Roux, B.; Nina, M.; Pomes, R.; Smith, J. C. Biophys J 1996, 71, 670.
20. Brooks, B. R.; Bruccoleri, R. E.; Olafson, B. D.; States, D. J.; Swaminathan, S.; Karplus, M. J Comput Chem 1983, 4, 187.
21. MacKerell, A. D., et al. J Phys Chem 1998, 102, 3586.
22. Nina, M.; Roux, B.; Smith, J. C. INSERM/John Libbey Eurotext Ltd. 1992, 221, 17.
23. Nina, M.; Smith, J. C.; Roux, B. J Mol Struct (Theochem) 1993, 286, 231.
24. Nina, M. Thèse de doctorat. Université Paris VI, (1994).
25. Ryckaert, J-P.; Ciccotti, G.; Berendsen, H. J. C. J Comp Phys 1977, 23, 327.
26. Van Gunsteren, W. F.; Berendsen, H. J. C. Mol Phys 1977, 34, 1311.
27. Interactive Data Language, Version 4; Research Systems Inc.: Boulder, CO, 1995.
28. ACM Trans. Math Soft 4, 148.
29. Wolfram, S.; Mathematica, Version 3; Wolfram Research Inc.: Champaign, IL.
30. Logunov, I.; Schulten, K. J Am Chem Soc. 1996, 118, 9727.